Semi-Annual Report
January - June 1995

Michael D. King and Si-Chee Tsay
Goddard Space Flight Center
Greenbelt, MD 20771

Abstract

Our major achievements of the past six months were: (1) studies of atmospheric correction (e.g., water vapor absorption and Rayleigh scattering) in MAS remote sensing retrievals, (2) distributions of a comprehensive ER-2 mission summary booklet for the MAST experiment for use by the science community, (3) analyses of some interesting ship track cases to be presented at the London MAST workshop, (4) submission of the MAS instrumentation paper for publication, and (5) successfully done in conducting a field experiment in the Arctic region as part of MODIS research activities.

I. Task Objectives

With the use of related airborne instrumentation, such as the MODIS Airborne Simulator (MAS) and Cloud Absorption Radiometer (CAR) in intensive field experiments, our primary objective is to extend and expand algorithms for retrieving the optical thickness and effective radius of clouds from radiation measurements to be obtained from the Moderate Resolution Imaging Spectroradiometer (MODIS). The secondary objective is to obtain an enhanced knowledge of surface angular and spectral properties that can be inferred from airborne directional radiance measurements.

II. Work Accomplished

a. MODIS-related Algorithm Study

The MODIS cloud retrieval algorithm integration (e.g., PGS Toolkit, API, etc.) for the MODIS Beta-3 delivery is nearly completed. Menghua Wang has been interactively working with the MODIS SDST to update the cloud retrieval algorithm and to test implemented code in our 'redback' SGI workstation. Some of SDP tools (e.g., open, reading, and writing) have been implemented and tested both in the MODIS SDST platform (modis-xl) and 'redback'. The error message function has also been implemented but yet to be tested.

The first comprehensive paper describing the details of the MAS instrumentation and prospective science has been completed and submitted to the *Journal of Atmospheric and Oceanic Technology* for publication (see section VI). The application of the MAS solar channels to the study of cloud properties was discussed in the paper and also shown in Figure 1. Calculations of liquid water cloud reflectance throughout the solar spectrum are shown in Fig. 1a for a wide variety of cloud droplet effective radii (a useful moment of the droplet size distribution) and for the cloud optical thickness (at 0.75 µm) of 16. Figure 1b shows the top-of-the-atmosphere (TOA) brightness temperature as a function of wavenumber (wavelength) from 600-3340 cm^{-1} (3-16.7 µm) for both clear and cloudy mid-latitude summer conditions with an ocean-like surface having a temperature of 294 K. Unit emissivity (zero reflectance), overhead sun, and a low-level water cloud of optical thickness 5 (at 0.75 µm) placed at an altitude between 1 and 1.5 km were assumed. Appropriate gaseous absorption (e.g., water vapor, carbon dioxide, ozone, and the infrared water vapor continuum) was also included. The MAS channel locations are indicated in the upper portion of Fig. 1. It is clear from Fig. 1a that reflectance measurements in the 1.6, 2.2, and 3.7 µm windows provide useful information on the cloud droplet size. Reflectance measurements in the visible wavelength region, in contrast, show little variation with droplet size and can thus be used to retrieve cloud optical thickness. The sensitivity of retrieving cloud optical thickness and effective radius from thermal infrared is weak, as shown in Fig. 1b. In the 3.7 µm window, both solar reflected and thermal emitted radiation are significant, though the use of reflectance for cloud droplet size retrieval is seen to be much more sensitive than the thermal component (note that, in either case, the thermal and solar signals must be separated to provide the desired component). This leads to an important subject - atmospheric correction.

An appreciable amount of time was spent on studying the effects of molecular (Rayleigh) scattering and water vapor absorption on our cloud retrieval algorithm. The Rayleigh optical thickness at 0.664 µm is about 0.044 which is about two orders of magnitude smaller than the cloud optical thickness. Assuming a two-layer atmosphere with molecules above the cloud layer, Menghua Wang simulated the upward reflectance at the TOA for this atmosphere-cloud-ocean system. For the MAS 0.664 µm band, the upward reflectance at the TOA was computed for the cases of a cloud optical thickness τ_c = 2, 4, 6, 8, 10, and 12 and solar zenith angles of 0° to 80° at step of 10°. Comparing the lookup library reflectance that was computed using a one-layer cloud layer with a flat ocean surface at the bottom, the %-difference of the reflectance is typically about 15% at τ_c = 2 to less than 1% at τ_c = 12. For the larger solar zenith angle $\theta_0 > 70°$, the %-difference was even greater because of enhanced multiple scattering contributions from air molecules. From these results, we conclude that without a Rayleigh correction in our cloud retrievals, the cloud optical thickness would be overestimated. Therefore, it is very important to remove the Rayleigh contribution (especially for optically thin cloud layers). The water vapor transmission (t) can be approximated accurately using the analytical expression $t(\theta) = \exp(-[CW_0/\cos\theta]^a)$, where constant C and a are wavelength dependent, and W_0 is the column water vapor loading in (g cm^{-2}). This formula ignores the effects of atmospheric temperature and pressure in the water vapor transmission computation. Comparing these transmissions with Lowtran-7 models for the 2.14 µm channel, the error is typically less than 0.5% for θ up to 60° for all Lowtran-7 model atmospheres.

Steve Platnick worked independently in developing Rayleigh reflection and transmission matrices for use in his adding code to determine the effect of Rayleigh scattering on cloud retrievals. The correlated k-distribution data developed by David Kratz at NASA Langley for MAS 3.7 and 11 µm bands were also used. For transmittances in 0.67, 1.6 and 2.2 µm channels, the MODTRAN results were adopted before the completion of Kratz's correlated k-distribution for MAS. This provides us with an independent comparison.

Platnick is also collaborating with the CERES Science Team at NASA Langley Research Center on providing a cloud retrieval code for use in their upcoming global AVHRR study. A great deal of time was spent on extensively modularizing, structuring, and documenting the retrieval code. This code includes a hard-wired atmospheric corrections for two different cloud tops, as input from other analyses. After completing the reflectance and emission libraries for the spectral bandpasses of AVHRR NOAA-9 and compared with previous NOAA-11 and 12 libraries, Platnick discovered that the effective variance of the drop size distribution (v_{eff}) is an important parameter. More sensitivity studies are underway.

b. MODIS-related Instrumental Research

After the first completion of the MAS 50-Channel Data Acquisition / Digitizer System (DAS), about 3 hours worth of data were collected on January 3, 1995. Jeff Myers at NASA Ames reported that all 50 channels appeared to be functioning, and the hardware performed well. Most of the IR channels were significantly cleaner than they were on the previous data system. The raw data look very strange, containing DC drift and digital gain / offset variations that must be removed during data post-processing. It is very tedious to examine all of these data immediately following flight using the newly developed "quick-look" system. Dave Augustine, in collaboration with Ames, continues to work on Quick-look display software for the 50-channel data system. This will allow the user to view the raw MAS data in either single channel, three channel simultaneous, or RGB composite modes; other options are an interactive stretch of the color tables (both upper and lower boundaries), tape manipulation (skip files, tape rewind, and position to selected scan) and custom color tables.

The performance of the MAS 50-channel instrument was first confirmed during Menzel's Houston experiment (January 5-20, 1995). The MAS and HIS (High-resolution Interferometer Sounder) were deployed together on the NASA ER-2 aircraft for 8 missions (including ferry flights to and from Houston). Initial investigation of the 50-channel MAS data revealed very good performance in all four ports. In particular, for port four there was roughly a three to four times improvement over the NEΔTs achieved during TOGA-COARE. One important thing left for this new MAS 50-channel is the format and structure of a new level-1B HDF file format and contents. This must be carefully designed, and of course calibration results available for all 50 channels, before producing a useful archival level-1B product.

Further performance evaluations of the MAS 50-channel were done in a Snow / Sea Ice Mapping Mission during April 3-24 and the ARMCAS (Arctic Radiation Measurement in Column Atmosphere-surface System) mission during June 1-15 (both based in Fairbanks, Alaska). Figure 2 shows high resolution images of a convective cumulonimbus cloud surrounded by lower level water clouds on the northern foothills of the Brooks Range, Alaska (69°7'N, 148°34'W), near the town of Sagwon, acquired on June 7, 1995. These panels are raw images consisting of 716 pixels cross-track and 716 scan lines along track, and are oriented from south (at the top) to north (at the bottom), where the ER-2 aircraft heading was 352°. The panel in the upper left (0.657 µm) shows high contrast between the optically thick (and therefore bright) cumulonimbus cloud, diffuse cirrus anvil, and remnants of the snow pack lying in ravines and topographic depressions (right center of image), less reflective altocumulus clouds (upper portion of image), and dark tundra. In contrast, the panel in the upper right (1.609 µm) shows that the cumulonimbus and cirrus anvil are composed of ice (low reflectance) and the surrounding altocumulus clouds are composed of water (high reflectance), as expected. The 1.879 µm panel in the lower left is especially sensitive to water vapor absorption in the atmosphere, and thus the high cumulonimbus and cirrus clouds are bright (little water vapor absorption above the cloud), whereas the lower-level altocumulus cloud and surface are darker due to absorption by water vapor in passing through a deeper atmospheric column. To support this interpretation, the 10.98 µm panel in the lower right appears quite cold (low intensity) in the coldest portion of the cumulonimbus cloud (–50°C), warmer at the top of the altocumulus cloud (–18°C), where the cloud must be composed of supercooled water rather than ice (according to the 1.609 µm channel), and warmest at the surface (+17°C). Figure 2 serves to illustrate the extraordinary capability, and quality, of the data produced by the MAS.

During the deployment of ARMCAS in Alaska, a MAS calibration meeting with Goddard and Ames personnel was held to discuss future plans for MAS calibrations. It was decided from this meeting that a more defined MAS calibration plan will be laid out for future missions, and more effort will be put into better understanding the temperature effects on the instrument, particularly in those conducted with the recently installed heater (after MAST). As a result of this meeting, the calibration plan includes: (1) standardizing calibration procedures, (2) gathering source calibration during field deployment, (3) performing cold chamber tests in a timely manner, and (4) coordinating final calibration documentation. Details of this plan will be drafted by Tom Arnold shortly.

All CAR calibration data for MAST (Monterey Area Ship Tracks, June 1994) and SCAR-C (Smoke, Clouds, and Radiation - California, September 1994) have been analyzed and preliminary calibration coefficients determined, based solely on the six-foot integrating sphere Feb-94 source calibration. Tom Arnold compared these data to the CAR calibration data for the 48-inch integrating hemisphere and showed excellent (<2%) agreement. Unfortunately, large changes in calibration (~20-30%) from the pre- to post-deployment (particularly for MAST) were observed. To account for these changes, the scan mirror was replaced by a freshly coated one and the telescope mirrors and accessible optics were cleaned by Nita Walsh. Then, the CAR was recalibrated with the hemisphere and the recorded data were processed though appropriate calibration software. The resulting coefficients differed significantly from the post-SCAR-C calibration but, as hoped, they agreed well with the pre-MAST coefficients. Thus, it is presumed that the 20-30% calibration change from pre- to post-MAST was due to degradation of the primary scan mirror surface. Max Strange made some modifications to the instrument panel box so that a new gain setting is temporarily held in memory and does not actually occur until the end of the active scan period.

The CAR was calibrated for ARMCAS using both the integrating hemisphere and sphere. Following the standard calibration procedures, other tests were conducted in front of the sphere to examine both the possible sphere loading errors and changes to the CAR signal due to changes in the size of the sample averaging region of each scan. Preliminary results from these tests show no noticeable loading problems or significant changes due to sampling size. The CAR geometry with respect to the calibration was reviewed by Tom and Nita and the results will go into a report on the history of CAR calibration.

c. MODIS-related Services

ARMCAS experiment

The ARMCAS was a small but focused field experiment designed to better understand the radiative processes in the Arctic. It is part of NASA's MTPE and MODIS cloud research activities, and involves close collaboration between NASA and the University of Washington's Cloud and Aerosol Research group (funded by NSF and ONR). The strategy for this experiment in the summertime Arctic included spaceborne remote sensing (polar orbiting satellites), high altitude remote sensing (NASA ER-2 aircraft at ~20 km), boundary layer *in situ* measurements (UW's C-131A aircraft), and surface remote sensing (various radiometers) and ground truth observations including radiosondes.

During June 1-15, 1995, Michael King, Tom Arnold, Dave Augustine, Jason Li, Steve Platnick and Si-Chee Tsay participated in the ARMCAS deployment. Work involving the NASA ER-2 aircraft, satellites and Operations Center were performed in the vicinity of Fairbanks, Alaska and work involving the UW C-131A aircraft and surface observations (NASA Code 923 scientists and NOAA personnel) were performed in the vicinity of Prudhoe Bay and Barrow. Figure 3 shows the general area interested (rectangular box with different rotations) and particular locations of operation. This mosaic of NOAA AVHRR images was produced during mid-summer, therefore the snow / ice line in the Arctic does not represent the sea ice boundary for early June. The science plan for this experiment is available.

The main objectives of ARMCAS were: (1) to collect cloud mask data for MODIS algorithm development, (2) to collect data for scale analysis at varying spatial resolutions, (3) to collect data for retrieving cloud properties over highly reflecting surfaces, (4) to obtain in situ measurements for cloud retrieval validation, (5) to measure droplet spectral absorption with cloud microphysics, (6) to measure aerosol light scattering and CCN properties, (8) to collect data for studying statistical properties of cloud microphysics, (9) to measure bidirectional reflectance of various surface types, and (10) to serve as a pilot study for the upcoming Arctic FIRE-III and SHEBA campaigns. ARMCAS consisted of various NOAA, DMSP and ERS satellites; the NASA ER-2 aircraft carrying the MAS, AVIRIS, RC-10, and CLS (Cloud Lidar System); the University of Washington's C-131A aircraft carrying a wide variety of instrumentation to measure atmospheric dynamics, thermodynamics, microphysics, chemistry and radiation (CAR); the surface team carrying the PARABOLA, sunphotometer, UV radiometer, broadband radiometers, spectrometer, and NOAA radiosondes.

During the entire experiment, 5 research flights were conducted by the ER-2 aircraft, which flew about 24 flight hours, and 10 research flights were conducted by the C-131A, which flew about 43 hours. Highlights of these flights are as follows:

- Preliminary results showed that all instruments onboard the ER-2 and C-131A aircraft, as well as surface instruments, were functioning well. The only exception was that the CLS did not collect data for 1 $^1/_2$ ER-2 missions due to a switch malfunction on the aircraft.
- All of the ER-2 missions performed a mapping grid pattern, consisting of 280 km parallel flight legs spaced 30 km apart, under which either the NOAA-12 (or -14) or ERS-1 satellites overflew.
- Two coordinated flights between the ER-2, C-131A and NOAA satellite were conducted for collecting cloud mask (multiple layer, water and ice clouds) and retrieval (low level, single layer water cloud) data.
- Five of the ER-2 missions (nine passes) and two of the C-131A missions overflew the ground-based sunphotometer sites on the tundra, many of which were under clear sky conditions.
- Four of the C-131A missions measured cloud microphysics with high frequency (26 Hz) for a long period of time at different levels.
- Three of the C-131A missions might well be in the diffusion domain.
- Five of the C-131A missions measured various types of surface bidirectional reflectance.
- The PARABOLA, surface radiometers and hand-held spectrometer col-

lected good to excellent data during five days at three sites, under both clear and completely overcast skies at solar zenith angle between 45° and 75°.

Meetings

1. Si-Chee Tsay attended the coordination meeting among NSF/ONR SHEBA, DOE/ARM NSA site, and NASA FIRE-III field programs, in conjunction with the AMS 75th Annual Meeting, Dallas, TX on January 15-20, 1995;

2. Si-Chee Tsay attended the DOE/ARM NSA site Instrument Team Meeting, Reston, VA on February 1 and gave a talk on "Measuring surface bidirectional reflectance;"

3. Michael King attended the Ocean Color Calibration/Validation Workshop at the University of Miami on February 22-24, and gave a presentation on the EOS calibration and validation program;

4. Michael King attended the Science Working Group for the AM Platform (SWAMP) meeting in Greenbelt, MD on March 1, and gave a presentation on the EOS calibration and validation program, and short term budgetary and programmatic pressures on NASA;

4. Si-Chee Tsay, Steven Platnick and Menghua Wang attended a one-day workshop with the CERES group at NASA Langley on March 6 to discuss collaboration between MODIS and CERES modeling and retrieval efforts;

5. Michael King and Si-Chee Tsay attended the SCAR-B Science Team Meeting, in conjunction with AGU Chapman Conference on Biomass Burning and Global Change, in Williamsburg, VA on March 12-13;

6. Michael King attended the DOE/ARM Science Team Meeting, San Diego, CA on March 20-23 and presented a paper entitled "Earth Observing System (EOS): Science Objectives & Validation Plans;"

7. Si-Chee Tsay, Steven Platnick and Menghua Wang attended the CERES Science Team Meeting at NASA Langley on April 19-21, gave a presentation of "A science plan on radiation measurements in the Arctic" by Si-Chee Tsay and "Atmospheric effects on the cloud retrieval algorithm: Model simulations" by Menghua Wang;

8. Tom Arnold attended the SIRREX-4 Workshop at NIST in Gaithersburg, MD on May 2-3 to discuss radiometric source calibrations traceable to NIST standards;

9. Michael King, Si-Chee Tsay, Steven Platnick, Robert Pincus and Menghua Wang attended the MODIS Science Team Meeting in Greenbelt, MD on May 3-5;

10. Michael King, Si-Chee Tsay and Robert Pincus attended the first FIRE-III Science Team Meeting in Baltimore, MD on May 30 - June 2, and Michael King presented both PIs' Science Objectives;

11. Si-Chee Tsay attended the SUCCESS and SHEBA Working Group Meetings in Baltimore, MD on May 30-31.

Seminars

1. King, M. D., "Clouds, Radiation and Climate from EOS," Geophysical Fluid Dynamics Laboratory, Princeton, NJ, January 13, 1995;

2. King, M. D., "Earth Observing System: Objectives and Challenges," Geophysical Institute, University of Alaska, Fairbanks, AK, June 9, 1995;

3. Tsay, S. C., "Arctic Radiation Measurements in Column Atmosphere-surface System," Geophysical Institute, University of Alaska, Fairbanks, AK, June 16, 1995;

4. Tsay, S. C., "Recent Development in Radiative Transfer Model and its Applications," Institute of Remote Sensing Application, Chinese Academy of Sciences, Beijing, China, June 21, 1995;

5. Tsay, S. C., "Remote Sensing and Retrieval of Cloud and Surface Properties," Institute of Atmospheric Physics, Chinese Academy of Sciences, Beijing, China, June 28, 1995;

6. Tsay, S. C., "Effects of Cloud Inhomogeneity on Atmospheric Energetics and Remote Sensing," Center for Climate System Research, University of Tokyo, Tokyo, Japan, July 3, 1995;

III. Data/Analysis/Interpretation

a. Data Processing

New 3.7 µm MAS channel images from the ASTEX experiment are now available on the World Wide Web. Jason Li has automated the procedure for producing the Mosaic GIF images from MAS-processed HDF data. The MAS 3.7 µm shortwave infrared channel is sensitive to cloud streaks generated by ship effluents. The Wild-Heerbrug RC-10 photographs, on the other hand, provide visual identification of the location of a ship for verification purposes. The combined RC-10 photograph and MAS 3.7 µm image contribute to a nice cover page for a paper that presents a summary of the MAST experiment (in preparation for *Bull. Amer. Meteor. Soc.*). To aid in the data analysis of each MAS (and others) mission, a considerable amount of time has been spent to construct an ER-2 Mission Summary booklet. The MAST experiment was selected to initialize the layout. The content of the MAST summary booklet includes a description of instrumentation contained on the ER-2 aircraft, a list of flight environmental conditions, mission summaries written by the ER-2 flight scientist on flight days, ground tracks flown by the ER-2, the MAS flight line summary for each flight, quick look images for an entire flight produced from MAS data, and summaries of the location and time of RC-10 camera photographs. This MAST summary booklet focuses primarily on MAS imagery, but also contains information on the RC-10 photography and availability of processed MAS data through the GSFC Distributed Active Archive Center (DAAC).

To aid in analyzing MAST data and validating our cloud retrievals, a flight track program was designed by Tom Arnold to plot both ER-2 and UW's C-131A flight tracks. For the C-131A flight tracks a dashed line is plotted for data when "in-cloud" (defined as FSSP liquid water content > 0.005 g m^{-3}) and a solid thin line is used for data when not "in-cloud." ER-2 tracks are plotted as a solid heavy line. Tracks are labeled with arrows every 10 minutes of flight and with a time code stamp at the start of each hour. Time series of various microphysical parameters (e.g., altitude vs. liquid water content, drop concentration, and effective radius) were processed for all MAST flights.

To standardize our data format, Jason Li and Ward Meyer are restructuring all CAR data sets to adopt the HDF format (EOSDIS data standard). In addition, the first stage data visualization tools for viewing data from CAR raw data and CAR HDF products have been completed. Furthermore, Li has successfully merged cloud microphysics data gathered by the University of Washington's C-131A into the CAR HDF test set with correct CAR-cloud microphysics time alignment. This CAR HDF test set is Flight 1478 of the Kuwait Oil Fire experiment. Dr. Robert Pincus, an NRC post-doctoral fellow joining the group in April, is focusing on fully utilizing this random-access and self-description capabilities of the new HDF file format, and on moving from a mainframe to a workstation environment. These activities should make it easier to systematically process large quantities of CAR data. The CAR data analyses involving diffusion domain and aerosol-radiation interaction are currently underway.

b. Analysis and Interpretation

Preliminary MAST data have been analyzed for June 11, 13, 16, 28, 29 , and 30. Ship tracks have been analyzed for three of those days (6/11, 13, and 29). Steve Platnick will present and discuss some of these results at the MAST Workshop in London.

Figure 4 summarizes current cloud retrievals using MAS 0.66 and 2.13 µm channels during MAST. For correcting the atmospheric influence, a two- to three-point coefficient fit is made to match the calculated MODTRAN transmittance (and emission, if appropriate) for mid-latitude summer conditions. As expected, the retrieved cloud optical thickness increases (Fig. 4a), and the effective particle radius decreases (Fig. 4b), in ship tracks, relative to pristine, noncontaminated clouds outside the ship tracks. By implementing a water vapor correction (twoway transmission) into Nakajima and King's cloud retrieval algorithm, the retrieved cloud effective particle radius and optical thickness for MAST on June 29 (Flight #7, scan line 1600 and 8000) were studied by Menghua Wang for various water vapor loadings. The corrected reflectances were compared with the lookup tables. The retrieved effective radius decreases with an increase in water vapor loading since the upward reflectance was increased. However, the retrieved effective particle radius inside the ship tracks was not sensitive to the water vapor loading. In analyzing MAST data, Platnick found that gradient search methods may not always be accurate for near-IR bands other than for the 3.7 µm channel. When the optical thickness is relatively small (e.g., ≈ 6) there may be a few local minima that, in turn, can lead to multiple solutions for both the 1.6 and 2.2 µm bands at realistic radii. Further study of this problem is currently underway.

The 3.7 µm susceptibility (not shown), defined as the increase in cloud reflectance for a one drop per cm^3 increase in droplet concentration, appears to be a relatively successful predictor of ship track strength. However, for most of these ship track days, the cloud structure and variability was large, making a correlation between ship track strength and 3.7 µm susceptibility much less than perfect (which is not expected to be exact due to dynamical effects). In addition, for most cases the liquid water path actually decreases in the ship track, rather than increases! Part of the reason for this appears to be the fact that visible reflectance does not change much in any of these tracks. So as r_e decreases, there is not enough corresponding increase in τ to keep the liquid water path constant, much less have it increase. Also, the underlying assumption of all this is that the retrievals are accurate, or at least have relative consistency. Much more work needs to be done on this and will take some careful statistical analysis.

Figure 5 shows the retrieved cloud optical thickness (Fig. 5a) and effective particle radius (Fig. 5b) for MAS two-channel analyses (pairs of MAS visible and each of three near-infrared channels) on MAST for June 11. The retrieved τ for three near-infrared channels is peaked at a larger optical thickness as the wavelength increases, which is in good agreement with the general trend of Mie computations for various size distributions in water clouds. The retrieved r_e (Fig. 5b) also shows a similar behavior, peaking around 5, 6, and 10 µm with increasing wavelength. Unlike the optical thickness, the effective radius is a physical parameter and should not have wavelength dependence. Quick comparison of these results with averaged C-131A FSSP microphysics data, one finds that the 2.13 µm retrieval appears to be low by about 1-2 µm. The 1.61 µm retrieval likewise appears too low, while the 3.74 µm retrieval is probably too high. These results may contain some information about the vertical structure of cloud microphysical inhomogeneity. More sensitivity studies of spectral dependence on vertically inhomogeneous microphysics and careful statistical analysis of in situ measurements at different cloud levels are needed to address this question. Another attempt at this problem may be the analysis of spectral features of the glory. During MAST, the MAS collected many glory observations. Detailed studies of these data are underway.

IV. Anticipated Future Actions

a. Continue to analyze MAS data obtained from the MAST field campaign and compare with in situ microphysics measurements in more detail;

b. Continue to study the implementation of atmospheric corrections in our cloud retrieval algorithm;

c. Start to analyze MAS, AVIRIS, and CLS data gathered during the ARMCAS campaign, as well as AVHRR, University of Washington's C-131A in situ and surface observation data to help develop cloud masking algorithm;

d. Continue to analyze surface bidirectional reflectance measurements obtained during the Kuwait Oil Fire, LEADEX, ASTEX and SCAR-A experiments;

e. Attend the MAST Science Team Workshop at London, UK on July 24-28, 1995 to present MAS data analysis on ship tracks;

f. Prepare and conduct the US-Brazil SCAR-B field campaign as part of the MODIS research activities, in Brasilia and other sites, Brazil during August 15-September 14, 1995;

g. Attend CERES and MODIS Science Team meetings at LaRC (September 20-22) and GSFC (November 14-17, 1995), respectively.

V. Problems/Corrective Actions

No problems that we are aware of at this time.

VI. Publications

1. King, M. D., D. D. Herring and D. J. Diner, 1995: The Earth Observing System (EOS): A space-based program for assessing mankind's impact on the global environment. *Opt. Photon. News*, **6**, 34–39.

2. Gumley, L. E., and M. D. King, 1995: Remote sensing of flooding in the US upper midwest during the summer of 1993. *Bull. Amer. Meteor. Soc.*, **76**, 933–943.

3. King, M. D., S. C. Tsay and S. Platnick, 1995: In situ observations of the indirect effects of aerosol on clouds. *Aerosol Forcing of Climate*, R. J. Charlson and J. Heintzenberg, Eds., John Wiley and Sons, 227–248.

4. Schwartz, S. E., F. Arnold, J. P. Blanchet, P. A. Durkee, D. J. Hofmann, W. A. Hoppel, M. D. King, A. A. Lacis, T. Nakajima, J. A. Ogren and O. B. Toon, 1995: Group report: Connections between aerosol properties and forcing of cli-

mate. *Aerosol Forcing of Climate*, R. J. Charlson and J. Heintzenberg, Eds., John Wiley and Sons, 251–280.

5. King, M. D., and M. K. Hobish, 1995: Satellite instrumentation and imagery. *Encyclopedia of Climate and Weather*, Oxford University Press (in press).

6. Wielicki, B. A., R. D. Cess, M. D. King, D. A. Randall and E. F. Harrison, 1995: Mission to Planet Earth: Role of clouds and radiation in climate. *Bull. Amer. Meteor. Soc.* (in press).

7. Tsay, S. C., M. D. King, and P. V. Hobbs, 1995: Arctic radiation measurements in column atmosphere-surface system - Science Plan. NASA GSFC internal report.

8. King, M. D., W. P. Menzel, P. S. Grant, J. S. Myers, G. T. Arnold, S. E. Platnick, L. E. Gumley, S. C. Tsay, C. C. Moeller, M. Fitzgerald, K. S. Brown and F. G. Osterwisch, 1995: Airborne scanning spectrometer for remote sensing of cloud, aerosol, water vapor and surface properties. Submitted to *J. Atmos. Oceanic Technol*.

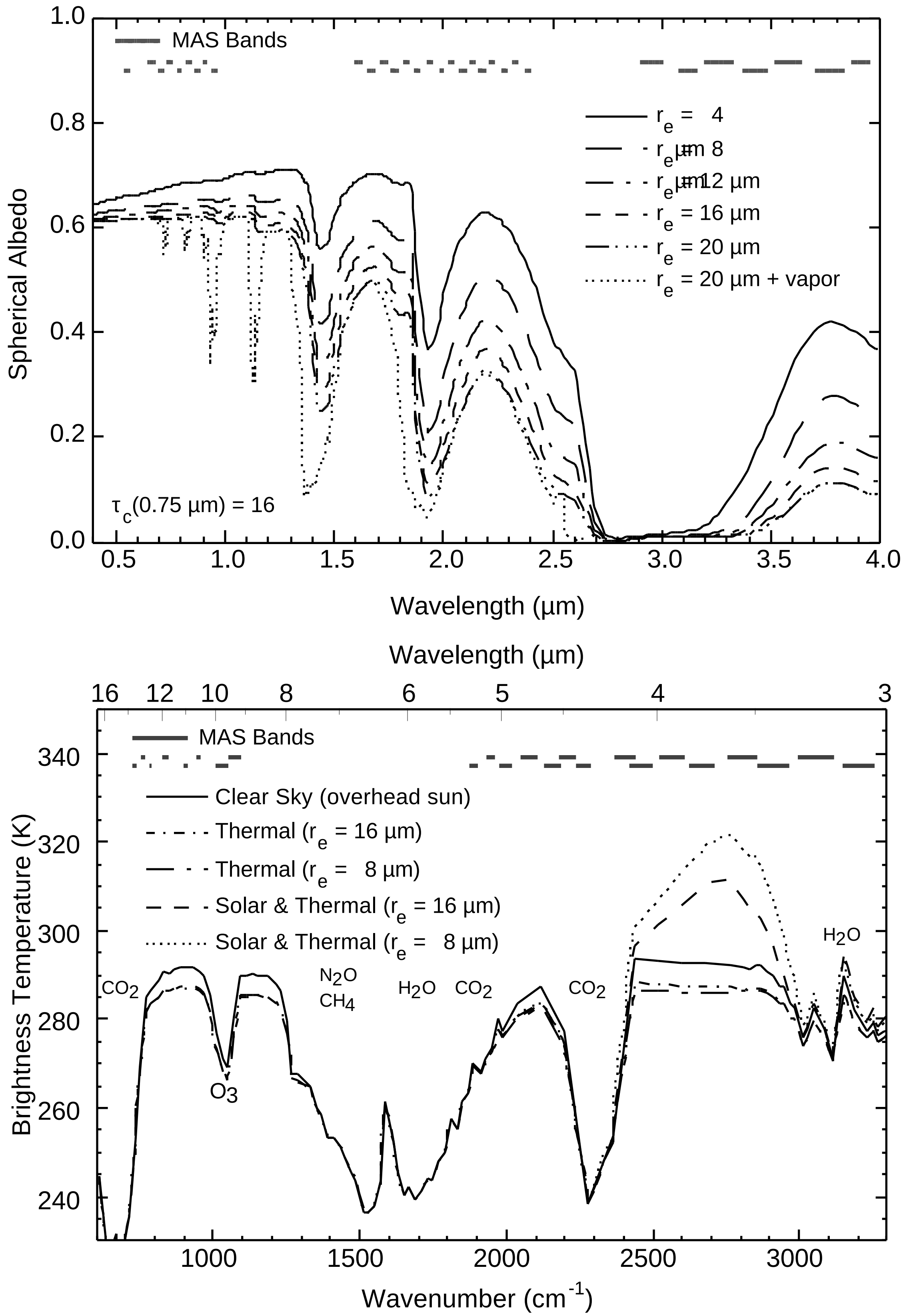
MAS Bands
re = 4
re µm 8
re µm 12 µm
re = 16 µm
re = 20 µm
re = 20 µm + vapor
τc(0.75 µm) = 16
Spherical Albedo
Wavelength (µm)
1.0
0.8
0.6
0.4
0.2
0.0
0.5
1.0
1.5
2.0
2.5
3.0
3.5
4.0
Wavelength (µm)
16
12
10
8
6
5
4
3
MAS Bands
Clear Sky (overhead sun)
Thermal (re = 16 µm)
Thermal (re = 8 µm)
Solar & Thermal (re = 16 µm)
Solar & Thermal (re = 8 µm)
CO2
O3
N2O
CH4
H2O
CO2
CO2
H2O
Brightness Temperature (K)
340
320
300
280
260
240
1000
1500
2000
2500
3000
Wavenumber (cm-1)

Figure 1

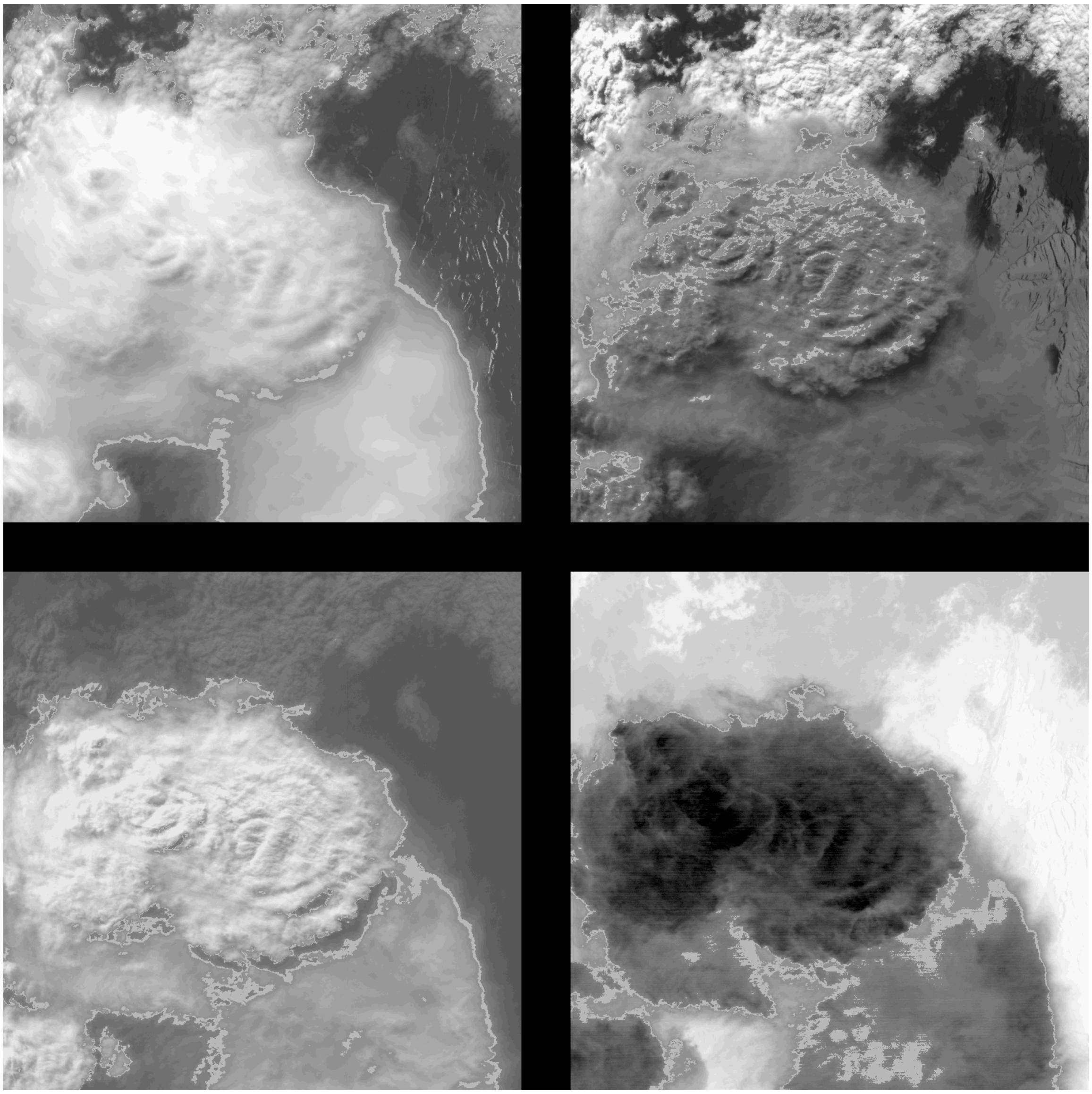

Figure 2

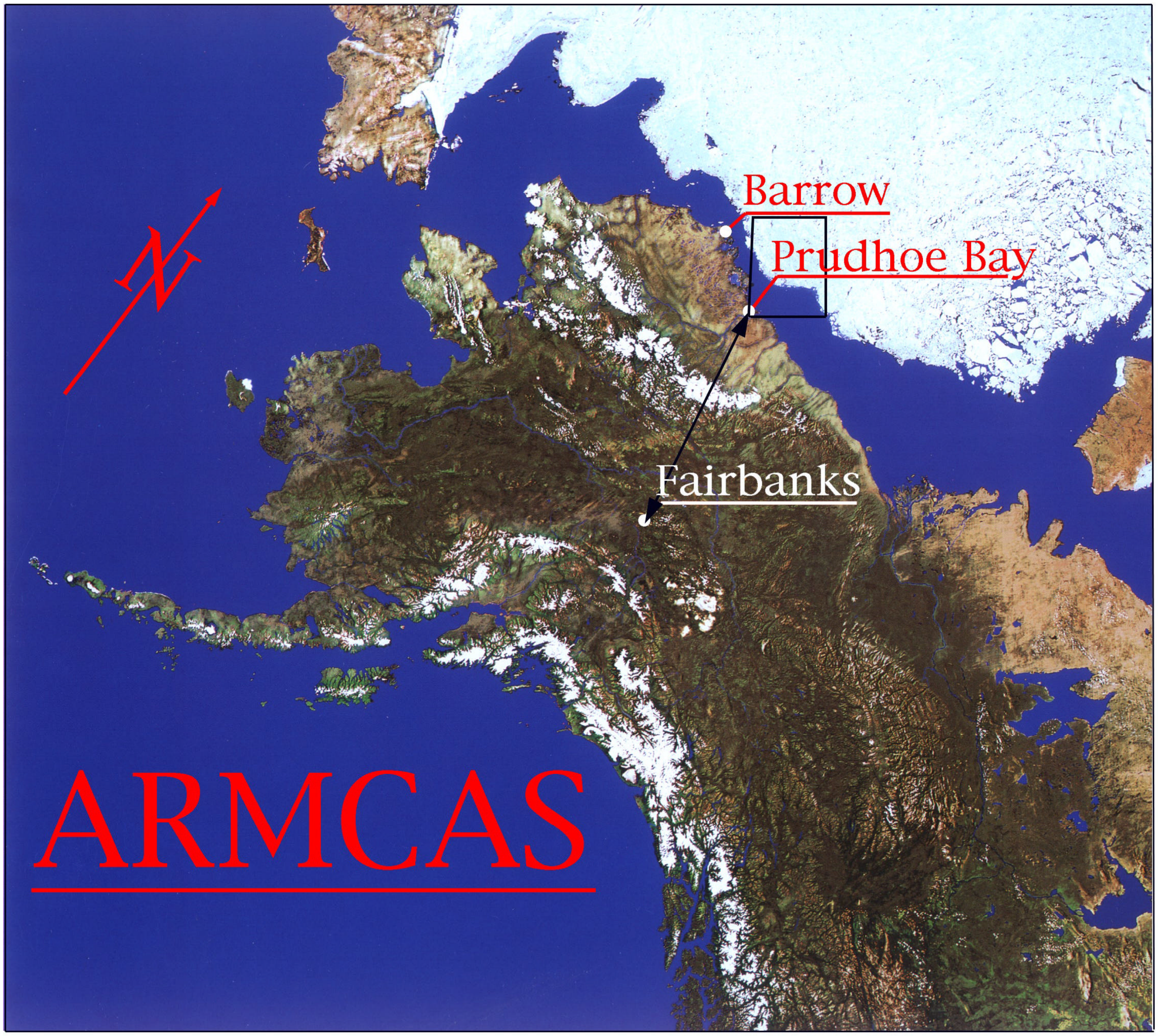

Science Plan

prepared at

NASA Goddard Space Flight Center

Figure 3

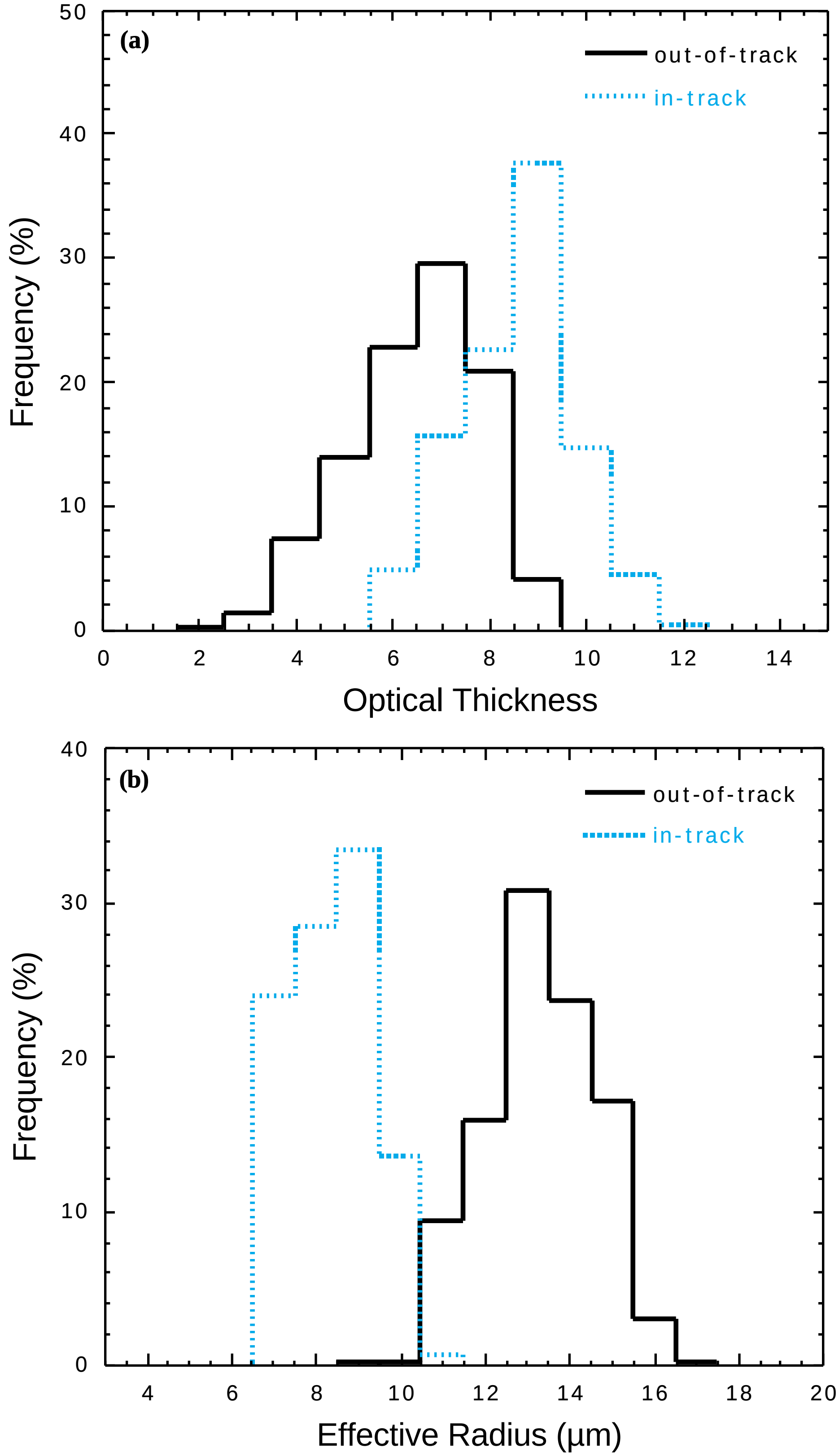
(a)
out-of-track
in-track
Frequency (%)
Optical Thickness
0
10
20
30
40
50
0
2
4
6
8
10
12
14
(b)
out-of-track
in-track
Frequency (%)
Effective Radius (μm)
0
10
20
30
40
4
6
8
10
12
14
16
18
20

Figure 4

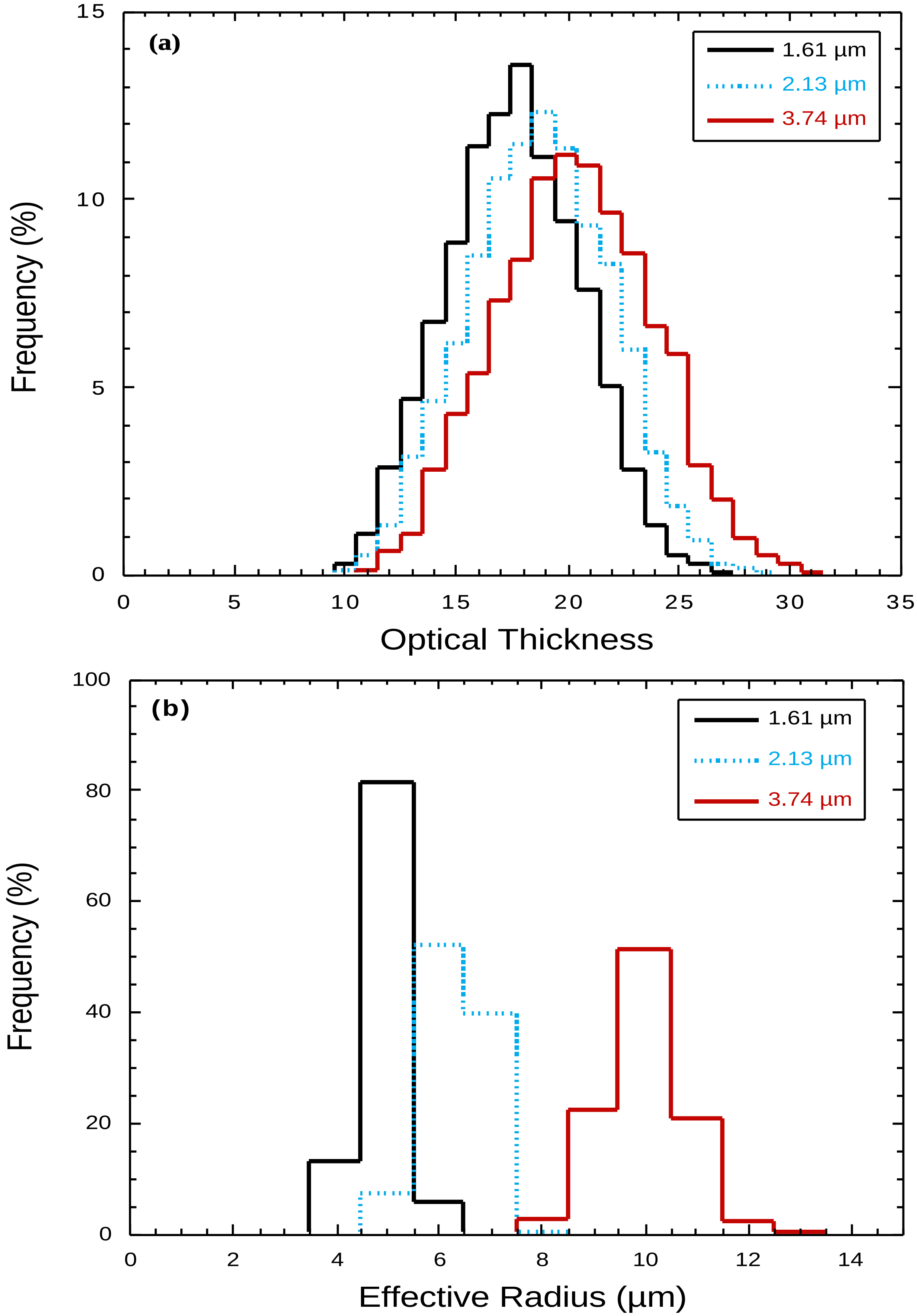

(a)
1.61 µm
2.13 µm
3.74 µm
Frequency (%)
0
5
10
15
0
5
10
15
20
25
30
35
Optical Thickness
(b)
1.61 µm
2.13 µm
3.74 µm
Frequency (%)
0
20
40
60
80
100
0
2
4
6
8
10
12
14
Effective Radius (µm)

Figure 5